Biosensors and Bioelectronics ■ (■■■■) ■■■–■■■

Contents lists available at ScienceDirect

Biosensors and Bioelectronics

journal homepage: www.elsevier.com/locate/bios

Nanoplasmonic biosensor: Detection and amplification of dual bio-signatures of circulating tumor DNA

Anh H. Nguyen, Sang Jun Sim*

Department of Chemical and Biological Engineering, College of Engineering, Korea University, Seoul 136-701, Republic of Korea

ARTICLE INFO

Article history:
Received 13 June 2014
Received in revised form
19 August 2014
Accepted 1 September 2014

Keywords:
Circulating tumor DNA
DNA methylation
Coupling gold nanoparticles
LSPR
Epigenetics
PIK3CA

ABSTRACT

Circulating tumor DNA (ctDNA) bearing tumor-specific mutation and methylation are promising biomarkers for noninvasive cancer assessment. However, existing methods for ctDNA detection are restricted to genetic mutations. Recently, nanoplasmonics has emerged as a platform for one-step dual detection with high sensitivity and specificity. Here we present a strategy for ultrasensitive detection of tumor-specific mutations (E542K and E545K) and methylation of ctDNA of *PIK3CA* gene based on localized surface plasmon resonance (LSPR) and the coupling plasmon mode of gold nanoparticles (AuNPs). Peptide nucleic acids (PNA) is used as a probe to capture and enrich the 69-bp *PIK3CA* ctDNA. The exposure of PNA-probed AuNPs to 200 fM ctDNA generates LSPR-peak shift of 4.3 nm, corresponding to the primary response. Immunogold colloids are exploited as methylation detectors and plasmon coupling based enhancement for secondary response. LSPR-peak shifted from 4.3 nm to 11.4 nm upon the immunogold colloids binding to two methylcytosines (mCpG), which is an approximately 107% increase, compared to that of the primary response. This enhancement leads to four times (~50 fM) improvement of sensitivity and because of two mCpG sites, ctDNA was detected. These results demonstrate that the sensor can simultaneously detect the hot-spot mutation and epigenetic changes on the ctDNA. Promisingly, other specific-tumor mutants and epigenetic changes can be detected at low concentration with this platform.

1. Introduction

Circulating tumor DNA, a double stranded DNA, represents a suitable biomarker (Dawson et al., 2013; Bader et al., 2006). ctDNA bearing tumor-specific sequence mutations and its epigenetic modifications are found in the cell-free fraction of blood, accounting for a variable, but small amounts of total circulating DNA (Sunami et al., 2009; Chimonidou et al., 2011). Mutation at two hot spots of E542K (G70271A in exon 9) and E545K (G70282A in exon 9) and methylation of ctDNA of *PIK3CA* (phosphatidylinositol 3-kinase catalytic subunit) are well-known mutations in many types of cancers including breast, colon, brain, liver, stomach, and lung (Bader et al., 2006; Banerji et al., 2012; Dawson et al., 2013; Lida et al., 2012; Wang et al., 2013). Development of a platform for dual biomarker detection of both genetic mutation and epigenetic alterations may increase the sensitivity and specificity of ctDNA-based diagnostics. As ctDNA sizes vary from 50 bp to 250 bp (Diehl et al., 2005, 2008; Jahr et al., 2001) and float in the cell-free streams, so capturing and enriching ctDNA targets are essential steps to completely eliminate unspecific binding.

As proof-of-concept, neutral-charged PNA molecules specifically hybridize with dsDNA, which makes it an outstanding probe for designing strand-specific dsDNA biosensors (Bhaskar and Bruce, 2001; Zohar et al., 2010). PNA molecules bind dsDNA with high affinity by the displacement mechanism which is stable in part due to a lack of electrostatic interference with the negatively charged phosphate backbone of DNA molecules (Zohar et al., 2010; Bentin et al., 2003). In particular, PNA/DNA mismatch is more destabilizing than a mismatch in a DNA/DNA duplex. For instance, a single mismatch in PNA/DNA and DNA/DNA complex decreases melting temperature 15 °C and 4 °C, respectively (Igloi, 1998; Ray and Nordén, 2000; Park et al., 2006). Therefore, PNA molecules can be ideal probes for DNA targets which eliminate false positive readouts on the sensor platform under thermally controlled conditions.

Two current strategies for quantification of tumor-specific mutations are digital PCR and targeted deep sequencing (Banerji et al., 2012; Board et al., 2008). Key obstacles of these techniques, however, are the need of labeling, the complicacy of operation, and the inability to dually detect the genetic mutation and methylation in one step. The sensor method with minimal sample, label-free,

* Corresponding author. Fax: +82 2 926 6102.
E-mail address: simsj@korea.ac.kr (S.J. Sim).

http://dx.doi.org/10.1016/j.bios.2014.09.003
0956-5663/

dual detection can be developed for recognition of genetic mutation and epigenetic alterations on the ctDNA molecules.

Notable nanoplasmonic gold nanoparticles (AuNPs)-based detection platforms can address various aforementioned obstacles, while preserving good sensitivity, specificity, and accuracy of the analytical assays. Many groups have worked out many different biosensing platforms to detect DNA targets via nanoplasmonic biosensors (Truong et al., 2011; Willets and Van Duyne, 2007; Ma et al., 2013). The principle of detection of the sensor relies on localized surface plasmon resonance (LSRP) which occurs when conduction electrons close the AuNPs surface sustain united oscillations coupled to a visible optical field (Fong and Yung, 2013; Willets and Van Duyne, 2007). The resonance of LSPR is dependent on the size, shape, and the surrounding dielectric environment of the AuNPs. This means that nanoplasmonic biosensors are refractometric nanosensors that are sensitive to alterations in the effective refractive index within the surface plasmon band (Brolo, 2012).

To the best of our knowledge,a biosensor for the dual detection for ctDNA has not been reported. Thus, we present a thermally-controlled plasmonics-based refractometric sensor to detect two bio-signatures of ctDNA: mutation at two hot-spots (E542K and E545K) and methylation (positions are shown in Supplementary information). Based on the thermal sensitivity of the PNA for mismatch binding, we designed the PNA probes with 100% matching for E542K and E545K mutant forms, with one mismatch for normal circulating DNA (ncDNA). mCpG sites on ctDNA being recognized by the immunogold colloids, which was simultaneously used to amplify the secondary LSPR signal. Beyond LSPR amplification, immunogold colloids are more sensitive by several hundreds of orders (Truong et al., 2013; Hall et al., 2011). In comparison with LSPR peak shape, amplified LSPR spectra due to plasmon coupling,exhibit a broader red-shift peak which can be observed (Lange et al., 2012; Zhao et al., 2014). As a result, the treatment of 200 fM ctDNA on the individual biosensor surface caused an LSPR peak shift at 4.3 nm. Then, after the use of the immunogold colloids a 107% increase (redder shift from 4.3 nm to 11.4 nm) in LSPR peak shift was observed and as a result of a set of simultaneous events two mCpG sites were detected and the detection sensitivity was increased 4 times from 200 fM to 50 fM of ctDNA. These results show that hot-spot mutations and epigenetic changes on the ctDNA were detected in one-step by the nanoplasmonic biosensor. It opens up a new approach for detection of ctDNA biosignatures at label-free, high sensitivity and specificity.

2. Materials and methods

2.1. Materials

PNA probes (5′-HS-AGTGATTTTAGAGAG- 3′) for hot-spot E542K and (5′-HS-CCTGCTTAGTGATTT-3′) for E542K, were purchased from Panagene, Korea. Synthetic 69-bp ctDNA (double strand) were purchased from Bioneer, Korea. Hydrogen tetrachloroaurate (III) trihydrate, trisodium citrate dihydrate, ascorbic acid, 1-ethyl-3-(3-dimethylaminopropyl) carbodiimide (EDC), N-hydroxysuccinimide (NHS), cetyltrimethylammonium bromide (CTAB), mercaptopropyltriethoxysilane (MPTES), human serum (H4522), phosphate buffer saline (PBS) (pH 7.4), $HS(CH_2)_{11}(OCH_2CH_2)_6OCH_2COOH$ (OEG_6), $HS(CH_2)_{11}(OCH_2CH_2)_3OH$ (OEG3), dithiothreitol (DTT), ethyl acetate, and ethanol were purchased from Sigma-Aldrich (USA). Milli-Q water with resistance at 18.2 mΩ/cm was used for all experiments.

2.2. Design PNA probes sequences and thermal-controlled capturing

The hot-spot mutants on ctDNA of *PIK3CA* gene were reported in previous papers (Bader et al., 2006; Dawson et al., 2013). The sequence of synthetic ctDNA containing the hot-spots is 69 bases long (Supplementary information). The 15 base-long probe was designed to match 100% for the target ctDNA from the 5′ and 3′ and to have a mismatch for the ncDNA. There is a big change (11 °C difference) in melting temperature of PNA probes for a mismatch for ncDNA and non-match for ctDNA. Recycled temperature ramping from 40 °C to 76 °C was to determine optimal binding between PNA and ctDNA, eliminate mismatch binding from ncDNA molecules at high temperature, and to enrich the ctDNA concentration. The results in thermal-controlled reaction chamber was measured by LSPR-peak shift, which reflected the presence of hot-spot mutations in ctDNA molecules.

2.3. Synthesis of gold nanoparticles and functionalization

50-nm gold nanoparticles were prepared as follows: reaction mixture of 10 mL of 0.1 M CTAB in water and 0.5 mL of 0.01 M $HAuCl_4$ in 1.0 mL of chilled 0.01$NaBH_4$ were added at high speed stirring (1300 rpm). The brown gold nanosphere suspension was formed under gentle heating, stirred for 10 min, and characterized using UV/vis spectroscopy (UV-3600, Shimadzu) and high-resolution transmission electron microscopy (TEM) (JEM-2100F, 200 kV, JEOL).

For PNA functionalization, the synthesized AuNPs (5.0 nM) in solution of 10% (v/v) Tween 10 in water (Duy et al., 2010) was readily functionalized with thiolated PNA probes overnight. The resulting mixture was then centrifuged at 10,000 rpm for 10 min and stored in 0.02% (v/v) Tween 20 in water for characterization using UV/vis spectroscopy.

2.4. Fabrication of the nanoplasmonic biosensor

To eliminate aggregation, the PNA-functionalized AuNPs were pretreated with 10% (v/v) Tween 20. The process of fabrication was conducted on closed bath imaging chamber (RC-30HV, Warner instruments). Briefly, we first immobilized the individual bare AuNPs (0.01 mg/ml) on the MPTES-functionalized glass (length of MPTES is 0.8 nm) which was inserted into the chamber, which was connected with the temperature controller (TC-324C, Warner Instrument). The 10% (v/v) Tween 20 in water was injected into the chamber to stabilize the AuNPs. Then, a mixture of thiol-PNA and oligo (ethylene glycol) with $HS(CH_2)_{11}(OCH_2CH_2)_6OCH_2COOH$ and $HS(CH_2)_{11}(OCH_2CH_2)_3OH$ (molar ratio 1:9) was used to exchange with CTAB, make spacers for PNA molecules, and block unspecific sites which could be reacted with DNA. The chamber was washed with PBS (pH 7.4). The PNA-functionalized AuNPs were ready for the detection of tumor-specific mutation and epigenetic alterations of ctDNA molecules.

The chamber subsequently was assembled onto the sample holder of the microscope and attached with a microsyringe pump (Harvard Apparatus). As shown in Fig. 1, the overall process of LSPR –based system uses a well-known biosensor including a dark-field microscope, spectrograph, and CCD camera, which has been described elsewhere (Truong et al., 2013; Willets and Van Duyne, 2007; Sagle et al., 2011). In brief, the dark-field microscope (Eclipse TE2000-U, Nikon) was used to illuminate scattered Rayleigh light from individual nanoparticles. The spectrograph (Microspec 2300i, Roper Scientifics) was connected with the microscope to collect the Rayleigh light scattering spectra, which was processed by a highly sensitive CCD camera (PIXIS: 400B, Princeton Instruments).

Please cite this article as: Nguyen, A.H., Sim, S.J., Biosensors and Bioelectronics (2014), http://dx.doi.org/10.1016/j.bios.2014.09.003

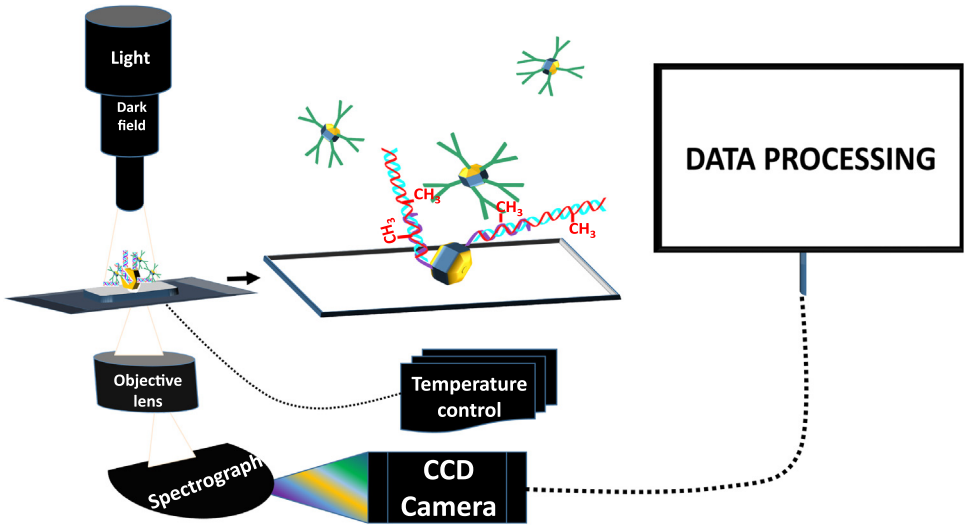

Fig. 1. Schematic diagram of fabricating nanoplasmonic biosensor for ctDNA and methylation detection. The graph showing the integrated system includes dark-field microscope, spectrograph, and CCD camera for illumination, collection, and signal conversion of Rayleigh scattering spectra. Upon binding of ctDNA molecules onto PNA probes, a distinct LSPR peak shift was generated, due to RI change. Methylation was detected and amplified by specifically binding immunogold colloids to methylated CpG sites on the ctDNA sequence.

69-bp target ctDNA molecules were captured and enriched on the biosensor surface. Due to different melting temperature, ncDNA was washed by PBS (pH 7.4) at 62 °C. The LSPR-based platform is very sensitive to refractive index (RI) changes surrounding the AuNP surface due to the binding of ctDNA. The shift index reflects the LSPR sensitivity of the sensor. To process the data, the Rayleigh light scattering spectra from individual AuNPs at different binding steps was recorded. The LSPR shift was calculated as follows: $LSPR_{shift} = LSPR_{after\ binding} - LSPR_{before\ binding}$.

2.5. Detection of circulating tumor DNA

Synthetic ctDNA with concentrations ranging from 50 fM to 3200 fM were prepared in mixture of 1X hybridization buffer (PerfectHyb™ buffer, Sigma): 1 × human serum (Sigma-Aldrich) was injected over the PNA-functionalized AuNPs, which were immobilized inside the chamber flow for 30 min. Temperature was controlled in the flow cell. Temperature was ramped to measure optimal binding of the PNA probes with the ctDNA target based on LPSR shift in real time; the optimal temperature was found to be 62 °C. Moreover, temperature ramping was also used to eliminate ncDNA binding. To ensure the LSPR shift due to specific binding between PNA probes and ctDNA, as well as to confirm the limit of detection (LOD), a control experiment was conducted by injecting 200 µl of 10 ng 69-bp *PIK3CA* DNA (normal case) and digested female human genome fragments (G1521, Promega, USA) over the biosensor surface in the flow cell for 30 min. After collecting the spectral map corresponding to each binding step, the LSPR shift was calculated as formulated above.

2.6. Preparation of anti-mC immunogold colloids

The AuNP surface was treated with thiol-oligo ethylene glycol (OEGs) for formation of the self-assembled monolayer (SAM), which reduces non-specific binding and stabilizes the gold solution: 8 ml of colloidal gold solution was mixed with 2 ml of 5 mM absolution ethanol solution containing OEG_6 and OEG_3 (1:9 M ratio) to get a final concentration of 0.5 mM. The reaction solution was centrifuged at 10,000 rpm for 20 min to remove unbound OEGs after 10-h of incubation. The sediment was re-suspended in deionized water and used in immunogold colloid preparation.

Stabilized AuNPs was pretreated with 1 M EDC/NHS to convert the carboxyl group of OEG6 to NHS esters, which can facilitate covalent bond formation with the carboxyl group of the anti-mC antibody. This reaction was terminated by adding 1.4 µl of 20 mM 2-mercaptoethanol. 500 µl (1 mg/ml) 5-methylcytosine (5-mC) monoclonal antibody (mAb) (Epigentek, USA) was subsequently added to the functionalized AuNPs. The immunogold (mAb-AuNPs) colloid was centrifuged at 10,000 rpm for 10 min after 3-h of incubating. The sediment was mixed in the 50 mM PBS buffer (pH 7.4) and stored at 4 °C for later use.

2.7. Methylation detection and LSPR spectra amplification

Two methylated mCpG sites exist on both strands of the ctDNA. After the primary response, methylation of ctDNA was detected and amplified using the mAb-AuNPs immunogold colloids. The immunogold colloids can amplify the resonant signal at ultralow concentrations of analytes (Truong et al., 2013; Hall et al., 2011). As shown in Fig. 1, the immunogold colloid solution was injected into the biosensor surface and incubated for 1 h to detect and enhance the signal. The surface was subsequently rinsed with deionized water and the amplified signal was measured by LSPR shift resonated by the immunogold colloids.

2.8. Reducing of false positive readouts

False positive readouts are virtually terminated by removing potential interferants from the sensing condition as well as the sample solution. We used temperature ramping rates to control the hybridization temperature on the biosensor surface between PNA probes with ctDNA (mutant) and ncDNA (wild type) in the acidic hybridization solulion (pH 5.4) with low NaCl concentration (10 mM) to solve the problems. The temperature ramping orderly includes: incubation at 40 °C for 30 min, increase of temperature to 75 °C (real-time measurement) (3 °C/min), elimination of denatured ncDNA from PNA probes by washing with deionized water and decreasing the temperature to 40 °C (3 °C/min). The optimal temperature for the efficient hybridization of ctDNA (100% match for PNA probes) and denatured ncDNA, was ready for LSPR measurements.

Please cite this article as: Nguyen, A.H., Sim, S.J., Biosensors and Bioelectronics (2014), http://dx.doi.org/10.1016/j.bios.2014.09.003

3. Results and discussions

3.1. Synthesis and functionalization of gold nanoparticles

Synthesized 50-nm gold nanoparticles for nanoplasmonic biosensor fabrication were directly confirmed using a TEM image (Fig. 2A) and a dark-field image of green scattering light (Fig. 2B), assigned to the plasmonic properties of AuNPs in the dark-field. 20 nm-gold nanoparticles for resonant immunogold colloids were purchased from Ted Pella, Inc. (USA) and re-imaged by TEM (Fig. 3A). Fig. 3B showed a shift of the plasmonic peak of the AuNP surface modification after each step. The wavelength shifted from 521 nm to 530 nm and to 534 nm corresponding to bare AuNPs, OEGs-functionalized AuNPs, and mAb-conjugated AuNPs, respectively. 9-nm redshift from 521 nm to 530 nm was observed when the OEGs were treated with 1.0 M DTT, which showed DTT-treated self-assembled monolayer of OEGs had a higher yield than a previous report (Cao et al. 2006). Conjugation of anti-methylcytosine antibody (mAb) via amid bonds on the OEG-functionalized AuNPs was observed with a 4 nm redder shift to 534 nm. This plasmonic damping was consistent with the previous reports, and shown a successful chemical modification of the AuNP surface (Truong et al. 2011; Sannomiya et al. 2008).

3.2. Nanoplasmonic biosensor for detection of circulating tumor DNA

PNA probes were designed for 100% matching with the ctDNA and mismatching with ncDNA. Optimal temperature for capturing the ctDNA was 62 °C. At this temperature, most of ncDNA molecules were melted from the biosensor surface since the melting temperature of the ncDNA was 54 °C (Fig. 4A). At first, 200 µl of 200 fM ctDNA or ncDNA was separately incubated with PNA-functionalized AuNPs which were immobilized the chamber at 40 °C for 2 h. The chamber was then washed with deionized water and LSPR peak shift was recorded at the highest hybridization. Subsequently, the temperature ramping was done from 40 °C to 76 °C to identify the melting temperature of PNA/ncDNA complex and then to determine a melting point to distinguish PNA/ctDNA and PNA/ncDNA hybridization. This is a very useful approach to reduce false positive readouts by elimination of ncDNA and another uncomplementary hybridization.

LSPR spectra shift indicated that ctDNA molecules were specifically captured on the PNA-probed AuNPs. The enrichment binding increased density of ctDNA on the surface and finally changed the refractive index which is a valuable factor for the LSPR-based biosensors. Temperature-dependent LSPR (Sagle et al., 2011) was determined in the range of 40 °C to 76 °C for LSPR shift compensation (Fig. 4A and Supplementary Fig. S2). Temperature-based LSPR-peak shift was stationary for ctDNA (about 5.9 nm) but decreased from 6.5 nm to 0.1 nm for ncDNA. Melting temperature for elimination of mismatch binding and other un-complementary binding was determined to be 54 °C, which was an important factor so as not to remove ncDNA and other DNA and to not disturb ctDNA hybridization on the sensor surface when clinical samples are used.

The single AuNP scattered a peak at 579.8 nm. After functionalization with OEGs, the LSPR peak shifted 13.7 nm to at 595.5 nm, which indicates a successful self-assembled monolayer (SAM) of OEGs on the AuNP surface. A 7.8 nm LSPR peak shift was generated by PNA probe conjugation on the functionalized AuNPs. After incubating 200 fM ctDNA in the flow cell containing individual nanoplasmonic biosensor for 30 min at 62 °C, a distinct Lorentzian-fitted LSPR-shift of 4.3 nm was observed compared to the previous step and with ncDNA addition (Fig. 4B). However, LSPR peak shift was not observed for the ncDNA molecules due to temperature control. Furthermore, when the temperature was decreased below 50 °C, peak shifts were observed in both of ncDNA and ctDNA (Fig. 4A). These results suggest that temperature is the key factor of selectivity, and the PNA probes exhibited good selectivity. Limit of detection (LOD) of ctDNA (primary detection, before amplification) was determined at 200 fM in range of 50–3200 fM, corresponding to the considerable LSPR peak shift of 4.3 nm (Fig. 5A and B).

3.3. Amplification of primary response signal and detection of methylation on ctDNA

Only 69-ctDNAs (E542K and E545K) of the *PIK3CA* gene contains two methylcytosine (mCpG) sites in the sequences (Sequence information, Supplementary information). To enhance the value of LOD from the primary detection and detect methylation on the ctDNA sequence, the 20-nm immunogold colloid solution was injected over the biosensor surface. The immunogold colloids bind onto mCpG sites on the ctDNA sequence and resonance of the LSRP spectra from the biosensor surface via plasmon coupling mode was shifted with a broad peak (Fig. 4B) (Lange et al., 2012). As a result, the immunogold colloids detected methylation at 2 mCpG sites on the ctDNA and showed a 107% increase from 4.3 up to 11.4 nm at the LOD value compared to that before the enhancement treatment (Fig. 5A). This enhancement value is not as high as reported 380% for lysozyme detection (Truong et al., 2013) and 400% for biotin and anti-biotin model (Hall et al., 2011). However, the enhancement depends on the density of the target on the biosensor surface (Cao et al., 2006; Truong et al., 2011), upon affinity of conjugated antibodies (Thakkar et al., 2013). To control the false positive readouts at the enhancement step, the primary response and enhanced assay were done at the same conditions (pH 5.4, 10 mM, 40 °C) for ncDNA in the range of 50–3200 fM.

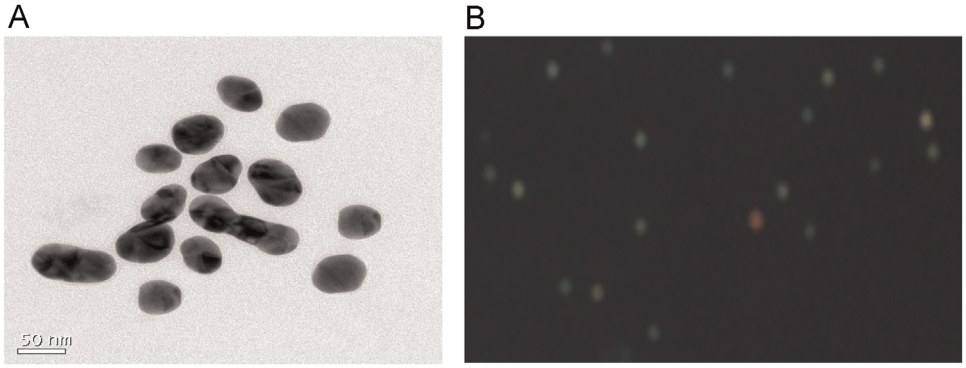

Fig. 2. (A) TEM image of 50-nm AuNPs and (B) wavelength selective scattering from 50-nm AuNPs observed by dark-field microscope at a magnification of 1500 ×. After properly being functionalized to capture ctDNA, these AuNPs were made into nanoplasmonic biosensors.

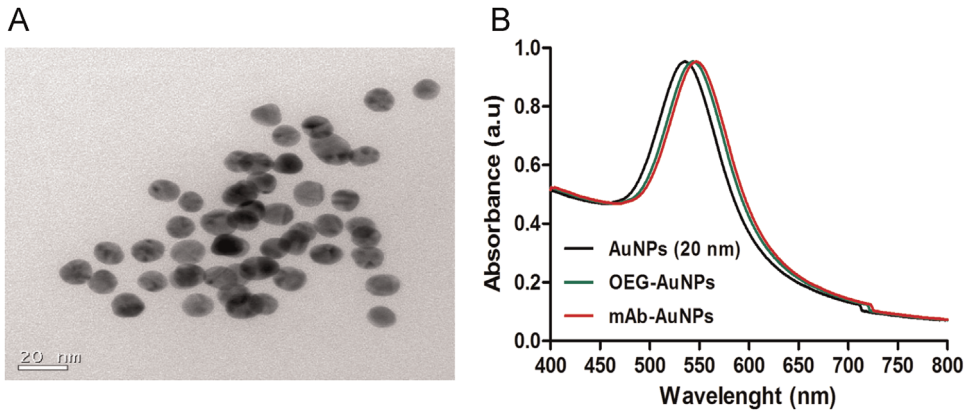

Fig. 3. (A) TEM image of 20-nm AuNPs for making immunogold colloids and (B) UV–vis spectra of AuNPs (521 nm), OEGs-functionalized AuNPs (530 nm) and mAb-conjugated AuNPs (534 nm).

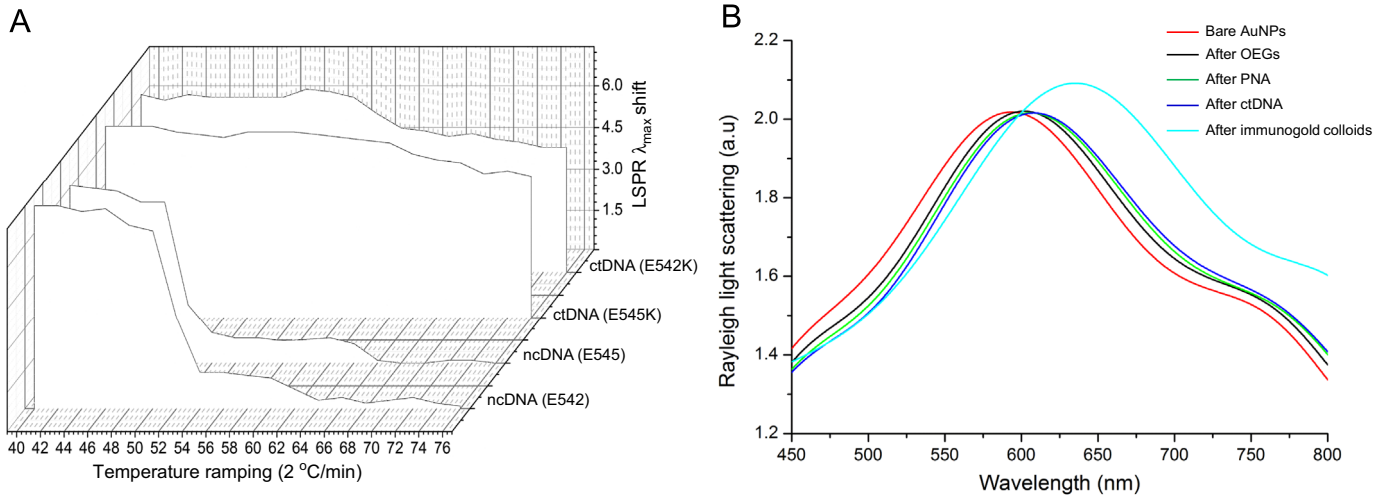

Fig. 4. (A) Temperature-dependent LSPR-shift for binding of the ctDNA molecules to PNA probes in real-time analysis, temperature helped selectively eliminate unspecific and mismatch binding. (B) LSPR-shift spectra of ctDNA binding and amplification of signal for methylation detection onto nanoplasmonic biosensor surface, fitted to Lorentzian algorithm after each step of the biosensing process.

No enhanced responses were observed from the primary response because there are no methylation sites on ncDNA (Fig. 5E). ncDNA molecules without epigenetic alterations are present at abundant concentration in the human serum (Chimonidou et al., 2011; Sunami et al., 2009).

As shown in Fig. 5A, the primary response (ctDNA detection) could not be detected at ctDNA concentrations below 50 fM and a calibration curve was fitted for concentrations higher than 50 fM (Fig. 5B). Moreover, the enhancement responds to two targets; (i) to amplify LSPR-peak shift of ctDNA detection and (ii) to detect methylation on ctDNA sequences. The red columns of Fig. 5A shows that methylated ctDNA can be detected at 2 mCpG sites with no ncDNA response (Fig. 5E). After injection of the immunogold colloids to detect the methylation on ctDNA, the binding event on the biosensor surface could be observed directly in the dark-field microscope (Fig. 5C and D). The relative LSPR-peak shift values of the ctDNA detection were enhanced considerably with the immunogold colloids based on the methylation of the ctDNA sequence. The logarithmic correlation between the relative LSPR-peak shift and ctDNA concentration (primary response), and enhanced response (methylation detection) exhibited the fitted linear correlation (Fig. 5B). In the fitted linear correlation, primary response indicated that the linear slope of LSPR-peak shift was lower than that of the enhanced assay because of saturation of binding sites on the AuNP surface (Sannomiya et al., 2008; Hall et al., 2011; Truong et al., 2013). Based on the slopes of the equations, it is obvious that the LOD of ctDNA was notably enhanced by the immunogold colloids specified for mCpG sites. In addition, the immunogold colloids did not bind to ncDNAs, resulting in a small change in the LSPR-peak shift (i.e., 2.1 nm). As a result, with the fabricated platform, we can detect both biosignatures including mutation at 50 fM ctDNA and two mCpG sites on the ctDNA of *PIK3CA* gene.

3.4. Detection of ctDNA from commercial Human serum samples

Serum ctDNA, tumor-specific genetic and epigenetic markers in cancer (Lavon et al., 2010; Dawson et al., 2013), are present at 5–720 copies/ml serum and account for 0.01% to 25% of normal circulating DNA (Dawson et al., 2013). Hence, a direct enrichment assay needs to perform on the binding chamber for real clinical serum samples before validation as a biosensor. Moreover, an enhanced assay needs to perform, as a sensor to detect epigenetic changes and to enhance the primary signal.

To mimic the clinical samples, we added 50 fM ctDNA of E542K and E545K into commercial human serum (H4522, Sigma-Aldrich) and injected the mixture into the biosensor which was controlled at 62 °C. It was a vital step to examine the biosensor capacity since real human serum samples contain various proteins and non-target DNAs in addition to the target ctDNA (Murtaza et al., 2013). Sensing target ctDNA at 62 °C, pH 5.4, with 10 mM NaCl, to eliminate ncDNA binding, non-target DNA, and physical binding

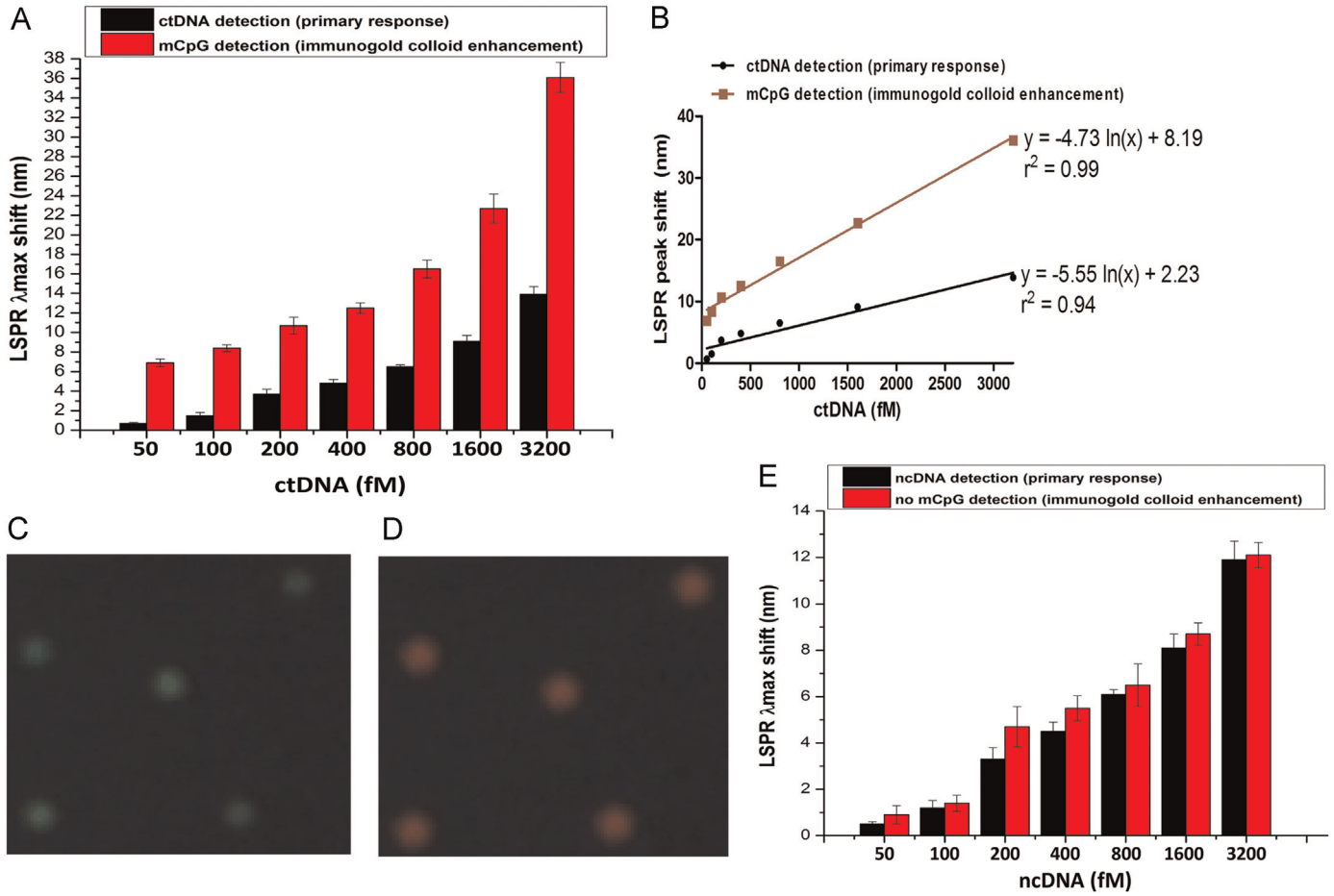

Fig. 5. (A) First detection of concentration of ctDNA ranging 50 fM to 3200 (black columns) and second detection and amplification for mCpG sites on ctDNA (red columns). (B) Linear-scale correlative analysis between LSPR shift and ctDNA concentration, methylation status on ctDNA. (C) Dark field image of AuNPs under ctDNA detection (before enhancement). (D) Dark-field image of AuNPs under methylation detection and enhancement (immunogold colloids). (E) No methylation detection and signal enhancement for un-methylated ncDNA. (For interpretation of the references to color in this figure legend, the reader is referred to the web version of this article.)

events by washing. After injection of the human serum samples, ctDNA E542K and ctDNA E545K were detected at 4.6 nm and 6.3 nm LSPR-peak shift, respectively. The biosensor surface was injected over with the immunogold colloids to detect methylation on the ctDNA and to amplify the primary response. The colloids specifically bind with two mCpG sites on the ctDNA to generate the enhanced signal at 11.8 nm and 15.7 nm for ctDNA E542K and ctDNA E545K, respectively (Fig. 6A and B).

The LOD was enhanced by four times of magnitude from 200 fM to just 50 fM and the LSPR-peak shift increased approximately 107% compared to the primary response by this enhancement. These results demonstrate that the nanoplasmonic

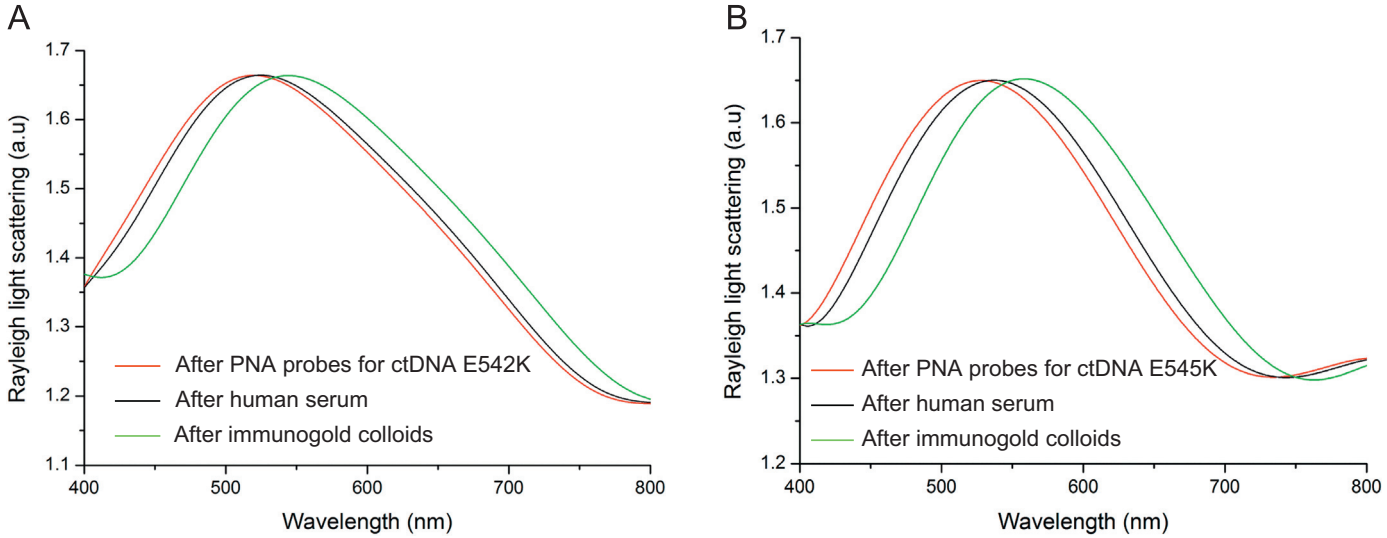

Fig. 6. Detection of ctDNA E542K and E545K in the pooled human serum at optimal conditions. Significant results were obtained for ctDNA E542K and E545K in the samples.

Please cite this article as: Nguyen, A.H., Sim, S.J., Biosensors and Bioelectronics (2014), http://dx.doi.org/10.1016/j.bios.2014.09.003

biosensor directly can detect ctDNA in the serum samples and the immunogold colloids can detect methylation on ctDNA & enhance the primary LPSR-peak shift. This also provided a potential approach to develop a platform based on coupling plasmonic mode for ultrasensitive and multiplex detection of inter-associated biological molecules.

4. Conclusions

We developed a PNA-based nanoplasmonic biosensor for detection of tumor-specific genetic and epigenetic markers of ctDNA of *PIK3CA* gene. Capturing and enrichment of ctDNA on the PNA-probed AuNP surface resulted in a change of the refractive index surrounding the biosensor surface, and was detected as distinct LSPR-peak changes on the Rayleigh light scattering. Moreover, we used the coupling plasmon mode of immunogold colloids to detect epigenetics changes and to enhance the primary signal of specific genetic mutations on the plasmonic biosensor. The enhancement assay amplified the signal four times lower LOD value and detected two mCpG sites on ctDNA. These results show that the nanoplasmonic biosensor can detect ctDNA in real clinical samples. This assay provides a sharp sensitive and multi-plexed platform for detecting not only ctDNA and its epigenetic changes, but also other associated biomarkers and their modifications at low concentration.

Acknowledgments

This work was supported by the National Research Foundation of Korea (NRF) grant funded by the Korea government (Ministry of Science, ICT & Future Planning) (Grant no. NRF-2013R1A2A1A01015644/2010-0027955), and the Korea CCS R&D Center grant funded by the Korea government (Ministry of Science, ICT & Future Planning) (Grant no. 2011-0031997) of the Republic of Korea.

Appendix A. Supplementary information

Supplementary data associated with this article can be found in the online version at http://dx.doi.org/10.1016/j.bios.2014.09.003.

References

Bader, A.G., Kang, S., Vogt, P.K., 2006. Proc. Natl. Acad. Sci. USA 103 (5), 1475–1479.
Banerji, S., Cibulskis, K., Rangel, E.C., 2012. Nature 486, 405–409.
Bentin, T., Larsen, H.J., Nielsen, P.E., 2003. Biochemistry 42, 13987–13995.
Bhaskar, D., Bruce, A.A., 2001. J. Am. Chem. Soc. 123, 9612–9619.
Board, R.E., Thelwell, N.J., Ravetto, P.F., Little, S., Ranson, M., Dive, C., Hughes, A., Whitcombe, D., 2008. Clin. Chem. 54 (4), 757–760.
Brolo, A.G., 2012. Nat. Photonics 6, 709–713.
Cao, C., Kim, J.P., Kim, B.W., Chae, H., Yoon, H.C., Yang, S.S., Sim, S.J., 2006. Biosens. Bioelectron. 21 (11), 2106–2113.
Chimonidou, A., Strati, A., Tzitzira, A., Sotiropoulou, G., Malamos, N., Georgoulias, V., Lianidou, E.S., 2011. Clin. Chem. 57 (8), 1169–1177.
Dawson, S.J., Tsui, D.W.Y., Murtaza, M., Biggs, H., Rueda, O.M., Chin, S.F., Dunning, M. J., Gale, D., Forshew, T., Betania, M.A., Rajan, S., Humphray, S., Becq, J., Dalsall, D., Wallis, M., Bentley, D., Phil, D., Caldas, C., Rosenfeld, N., 2013. N. Engl. J. Med. 368, 1199–1209.
Diehl, F., Li, M., Dressman, D., He, Y., Shen, D., Szabo, S., Diaz, L.A., Goodman, S.N., David, K.A., Juhl, H., 2005. Proc. Natl. Acad. Sci. USA 201, 16368–16373.
Diehl, F., Schmidt, K., Choti, M.A., Romans, K., Goodman, S., Li, M., Thornton, K., Agrawal, N., Sokoll, L., Szabo, S.A., 2008. Nat. Med. 14, 985–990.
Duy, J., Connell, L.B., Eck, W., Collins, S.D., Smith, R.L., 2010. J. Nanopart. Res. 12, 2363–2369.
Fong, K.E., Yung, L.Y., 2013. Nanoscale 5 (24), 12043–12071.
Hall, W.P., Ngatia, S.N., Duyne, R.P.v., 2011. J. Phys. Chem. C 115 (5), 1410–1414.
Igloi, G.L., 1998. Proc. Natl. Acad. Sci. USA 95, 8562–8567.
Jahr, S., Hentze, H., Englisch, S., Hardt, D., Fackelmayer, F.O., Hesch, R.D., Knippers, R., 2001. Cancer Res. 6, 1659–1665.
Lange, H., Juárez, B.H., Carl, A., Ritcher, M., Bastús, N.G., Weller, H., Thomsen, C., Klitzing, R.v., Knorr, A., 2012. Langmuir 28, 8862–8866.
Lavon, I., Refael, M., Zelikowitch, B., Shalom, E., Siegal, T., 2010. Neuro Oncol. 12 (2), 173–180.
Lida, S., Kato, S., Ishiguro, M., Matsuyama, T., Ishikawa, T., Kobayashi, H., Higuchi, T., Uetake, H., Enomoto, M., Sugihara, K., 2012. Oncol. Lett. 3, 565–570.
Ma, W., Kuang, H., Xu, L., Ding, L., Xu, C., Wang, L., Kotov, N.A., 2013. Nat. Commun. , http://dx.doi.org/10.1038/ncomms3689.
Murtaza, M., Dawson, S.J., Tsui, D.W., Gale, D., Forshew, T., Piskorz, A.M., Parkinson, C., Chin, S.F., Kingsbury, Z., Wong, A.S., Marass, F., Humphray, S., Hadfield, J., Bentley, D., Chin, T.M., Brenton, J.D., Caldas, C., Rosenfeld, N., 2013. Nature 497 (7447), 108–112.
Park, H., Germini, A., Sforza, S., Corradini, R., Marchelli, R., Knoll, W., 2006. Biointerphases 1 (4), 113–122.
Ray, Arghya., Nordén, B., 2000. J. Fed. Am. Soc. Exp. Biol. 14 (9), 1041–1060.
Sagle, L.B., Ruvuna, L.K., Ruemmele, J.A., Van-Duyne, R.P., 2011. Nanomedicine 6, 1447–1462.
Sannomiya, T., Hafner, C., Voros, J., 2008. Nano Lett. 8 (10), 3450–3455.
Sunami, C., Vu, A.T., Nguyen, S.L., Hoon, D.S., 2009. Methods Mol. Bio. 507, 349–356.
Thakkar, S., Kharade, N.N., Celkel, R., Peterson, E.C., Varughese, Kottayil., 2013. Sci. Rep. 4 (http://dx.doi.org/10.1038/srep03673).
Truong, P.L., Choi, S.P., Sim, S.J., 2013. Small 9 (20), 3485–3492.
Truong, P.L., Cao, C., Park, S., Kim, M., Sim, S.J., 2011. Lab Chip 11, 2591–2597.
Wang, W.F., Xie, Y., Zhou, Z.H., Qin, Z.H., Wu, J.C., He, J.K., 2013. Acta Pharmacol. Sin. 34, 1560–1567.
Willets, K.A., Van Duyne, R.R., 2007. Annu. Rev. Phys. Chem. 58, 267–297.
Zhao, Y., Xu, L., Ma, W., Wang, L., Kuang, H., Xu, C., Kotov, N.A., 2014. Nano Lett. 14, 3908–3913.
Zohar, H., Hetherington, C.L., Bustamante, C., Muller, S.J., 2010. Nano Lett. 10, 4697–4701.